

Local structure and site substitution in $\text{Al}_{86}\text{Ni}_6\text{Co}_2\text{Y}_{4.5}\text{La}_{1.5}$ bulk amorphous alloy

Y. Liu¹, G. Schumacher¹, I. Zizak¹, A. Erko¹, J. Banhart^{1,2}

¹Helmholtz-Zentrum Berlin für Materialien und Energie,
Hahn-Meitner Platz 1, 14109 Berlin, Germany

²Technische Universität Berlin, Materials Science and Technology,
Hardenbergstr. 36, 10623 Berlin, Germany

Abstract

The local structures around nickel and cobalt atoms in $\text{Al}_{86}\text{Ni}_8\text{Y}_6$ and $\text{Al}_{86}\text{Ni}_6\text{Co}_2\text{Y}_{4.5}\text{La}_{1.5}$ bulk amorphous alloys were measured by X-ray absorption spectroscopy. Strong bond-shortening and a concomitant reduction of nearest neighbours of Ni and Co were observed. The local structure around Ni is the same as that around Co which is attributed to site substitution of Ni by Co atoms in the amorphous structure. The configurational entropy is estimated to be the main thermodynamic driving force for the increase in glass forming ability when substituting Ni by Co and Y by La. The cluster-line model is not supported by our results.

Aluminium-based amorphous alloys containing both transition metals (TM) and rare-earth elements (RE) promise excellent mechanical properties such as high strength and corrosion resistance and are therefore of practical interest [1, 2]. Currently known Al-based amorphous alloys exhibit only moderate glass forming ability (GFA), partly ascribed to the fact that their glass forming range lies on the solute-rich side of the eutectic point, where the liquidus temperature rises steeply with Al concentration, resulting in a strongly reduced glass transition temperature [3]. Recently, the composition of an Al-rich Al-Ni-Y alloy with high GFA has been predicted using the cluster line model [4, 5]. This model assumes pronounced short-range order (SRO) around both Ni and Y atoms in the alloy. This SRO is described by local clusters with Ni or Y at their centres [5]. The numbers of Al nearest neighbours (coordination number, N) of Ni and Y was taken from ab-initio simulations based on density functional theory [6]. The composition of the alloy having the best GFA in the three-component Al-Ni-Y alloy system was determined by the intersection of the two cluster lines, the composition of each being determined by the number of nearest neighbours given by the atomic radii of the corresponding elements. The coordination numbers of 9.4 for Ni and 16.9 for Y taken from Ref. 6 yielded an alloy with composition $\text{Al}_{85.8}\text{Ni}_{9.1}\text{Y}_{5.1}$ [5] in reasonable agreement with the composition $\text{Al}_{86}\text{Ni}_8\text{Y}_6$ which was determined experimentally to possess the highest thickness of rods produced by injection of molten Al-Ni-Y alloys into the cavity of a copper mold. The GFA of $\text{Al}_{86}\text{Ni}_8\text{Y}_6$ was found to be high compared to most other Al-based amorphous alloys, and could be further improved by partial substitution of Ni by Co and of Y by La [4, 5]. Due to their similar metallic radii ($r_{\text{Ni}} = 124.6$ pm, $r_{\text{Co}} = 125.1$ pm [7]) and their similar electronic structure, the substitution of Ni by Co atoms in $\text{Al}_{86}\text{Ni}_8\text{Y}_6$ should cause only minor distortions in the local structure.

X-ray absorption spectroscopy (XAS) is known to be a useful tool to study the local structure in Al-based amorphous alloys. Furthermore, the determination of the coordination number in both $\text{Al}_{86}\text{Ni}_8\text{Y}_6$ and $\text{Al}_{86}\text{Ni}_6\text{Co}_2\text{Y}_{4.5}\text{La}_{1.5}$ alloys provides additional information on

the cluster structure in these alloys, and also on the optimum composition with respect to the GFA of these alloys. We therefore used XAS to study the local structure around Ni and Co atoms in $\text{Al}_{86}\text{Ni}_6\text{Co}_2\text{Y}_{4.5}\text{La}_{1.5}$ bulk metallic glass (BMG) in order to gain insight into the nature of element substitution.

Alloy ingots of nominal composition $\text{Al}_{86}\text{Ni}_8\text{Y}_6$ and $\text{Al}_{86}\text{Ni}_6\text{Co}_2\text{Y}_{4.5}\text{La}_{1.5}$ were produced by jointly melting the elements in a high frequency induction furnace under a purified argon atmosphere. Amorphous specimens of about 50 μm thickness were produced by rapid quenching from the melt using a splat quencher. The amorphous nature of the samples was verified by X-ray diffraction (XRD) using $\text{Cu-K}\alpha$ radiation and by transmission electron microscopy (TEM). Broad diffuse intensity maxima at $2\theta \sim 38^\circ$ are visible in the corresponding XRD patterns of the alloys. Analysis of the structure in a Philips CM30 transmission electron microscope (TEM) also revealed only broad diffuse intensity maxima, confirming the glassy nature of the alloys. Thermal stability was measured under a stream of argon gas by differential scanning calorimetry (DSC) during continuous heating with a heating rate of 20 K/min. The DSC traces of both the alloys $\text{Al}_{86}\text{Ni}_8\text{Y}_6$ and $\text{Al}_{86}\text{Ni}_6\text{Co}_2\text{Y}_{4.5}\text{La}_{1.5}$ reveal endothermic reactions prior to the first crystallization stage.

The local atomic structure of the samples was investigated by XAS at the bending-magnet beamline KMC-2 at the synchrotron radiation source BESSY-II in Berlin, Germany. Extended X-ray absorption fine structure (EXAFS) data were collected around both Ni and Co K-edges in the fluorescence mode. Appropriate reference foils of the pure elements Ni or Co were measured simultaneously with the amorphous alloy samples to provide an accurate energy calibration of the monochromator. The measured EXAFS spectra were transformed into k-space using the standard software combination ATHENA/ARTEMIS [8]. The structural data needed for calculating the fitting standards were prepared by applying the ATOMS code [9], while the theoretical scattering paths were calculated with the ab-initio software FEFF [10]. A single-shell model was fitted to the data in order to determine the number of nearest

neighbours N , the interatomic distance D , and the mean squared relative displacement of the effective interatomic distance σ^2 . For all the spectra, the single-shell model represented the data better than an fcc-structure. For Ni, an experimentally determined value of the amplitude reduction factor $S_o^2 = 0.9$ [11] was used. For Co the same value of S_o^2 was chosen as for Ni, because atoms with similar nuclear charge have similar S_o^2 values [12].

The Fourier-transform (FT) of the k^2 -weighted EXAFS signals in $Al_{86}Ni_6Co_2Y_{4.5}La_{1.5}$ for Ni and Co spectra are shown in Fig. 1 along with the corresponding fits to the data. For comparison, the FT of $k^2 \cdot \chi(k)$ measured at the Ni edge in $Al_{86}Ni_8Y_6$ is presented in Fig. 1c. None of the spectra are wave shift corrected. All three have a similar qualitative appearance. They reveal a maximum near $R = 2 \text{ \AA}$ and above $R \approx 2.5 \text{ \AA}$ $FT(k^2 \cdot \chi(k))$ does not reveal any distinct features. Here, the distance of the atoms varies strongly, indicating the lack of structural correlations beyond the first shell. The (phase-shift corrected) fit parameters are listed in Table 1. Within the experimental uncertainty, the number N of Al nearest neighbours, the distance D_{TM-Al} of the Al nearest neighbours and the mean squared relative displacement of the effective interatomic distance σ^2 , of both the Co and the Ni edge EXAFS are all equivalent between the two alloys. Therefore, the local structure around Ni and Co is concluded to be the same in $Al_{86}Ni_6Co_2Y_{4.5}La_{1.5}$. Moreover, the local structures around Ni in $Al_{86}Ni_6Co_2Y_{4.5}La_{1.5}$ and $Al_{86}Ni_8Y_6$ are the same. These similarities in local structure are ascribed to the nearly identical atomic radii of Ni and Co and to the similarity in their electronic structures reflecting similar electronegativities (1.91 for Ni and 1.88 for Co [13]) and similar negative mixing enthalpies with Al ($\Delta H_{mix}(Ni-Al) = -22 \text{ kJ/mol}$, $\Delta H_{mix}(Co-Al) = -19 \text{ kJ/mol}$ [14]).

According to Table 1, $N \approx 6$ for Ni and Co in both alloys. This value is about half the value $N_{DRPHS} \approx 11$ for both Ni and Co obtained by applying the dense random packing of hard spheres (DRPHS) model [15] to the metallic atomic radii given in Ref. [7]. Additionally, the bond lengths of the Al-Ni and Al-Co pairs, D_{Ni-Al} and D_{Co-Al} , are appreciably smaller than the

sum of the metallic atomic radii $r_{\text{Al}} + r_{\text{Ni}}$ and $r_{\text{Al}} + r_{\text{Co}}$, see Table 1, reflecting bond-shortening due to s-p hybridization: electrons with s-p character of Al are transferred to the d-states of the TM [16]. The strong bond-shortening is also indicated by the small effective radii r_{TM} and by the large values of r_{Al} (see Table 1) obtained by applying the DRPHS model to the experimentally determined values of N and D .

This interpretation, bond-shortening due to charge transfer from Al atoms located in the first coordination shell around the TM atoms, is supported by X-ray absorption near edge spectroscopy (XANES) of Ni and Co in $\text{Al}_{86}\text{Ni}_6\text{Co}_2\text{Y}_{4.5}\text{La}_{1.5}$, see Fig. 2. The onset of the absorption edges are shifted to lower values compared to the data of the corresponding reference specimens. This shift in XANES data is attributed to charge transfer from Al atoms to TM atoms, which is understood to be the origin of the resulting covalent character of the bonds and the reduced bond lengths. Shortening of Ni-Al and Co-Al bonds along with anomalously low coordination numbers ($N = 5.1 - 5.9$) has been observed in several amorphous Al-Ni-RE and Al-Co-RE alloys [16-19] and has been explained by the strong covalent character of these bonds.

The consequences of the notable covalent character of the bonds are evident. First, the strong covalent bonds between the “glue atoms” Ni and Co might at least partly be responsible for the high strength of Al-based amorphous alloys. Second, the covalent bond character leads to a strong reduction from $N \sim 11$ to $N \sim 6$ which differs appreciably from the values obtained by Sheng et al. [6] by ab-initio calculations for Ni ($N = 9.4$) and Co ($N = 9.4$) in $\text{Al}_{89}\text{Ni}_5\text{La}_6$ and $\text{Al}_{85}\text{Y}_8\text{Ni}_5\text{Co}_2$. Similar calculations were done for Y [6] resulting in $N(\text{Y}) = 16.9$. The use of the coordination number of Ni obtained from our EXAFS analysis in combination with the cluster line model and using $N(\text{Y}) = 16.9$ yields an alloy composition $\text{Al}_{81.6}\text{Ni}_{13.6}\text{Y}_{4.8}$. This differs appreciably from the composition reported by Yang et al. [4, 5], which was reported to have optimum GFA in the Al-Ni-Y alloy system. Hence, our results suggest, that the use of more realistic values of $N(\text{Ni})$ along with the cluster line model does

not yield a composition with optimum GFA and, therefore, does not support the cluster line model. Third, the large differences between the effective radii and the metallic radii of Ni, Co and Al in $\text{Al}_{86}\text{Ni}_6\text{Co}_2\text{Y}_{4.5}\text{La}_{1.5}$ suggest that structure models based on the DRPHS must be checked with respect to their applicability to Al-based glassy alloys and other glasses with strong covalent character of the bonds.

In order to study the influence of the element substitution on the GFA we estimated for $\text{Al}_{86}\text{Ni}_8\text{Y}_6$ and $\text{Al}_{86}\text{Ni}_6\text{Co}_2\text{Y}_{4.5}\text{La}_{1.5}$ the Gibbs free energy of mixing ΔG_{mix} given by:

$$\Delta G_{mix} = \Delta H_{mix} - T \cdot \Delta S_{mix} \quad (1)$$

where ΔH_{mix} denotes the increment in the mixing enthalpy and ΔS_{mix} the increment in the mixing entropy, adopting the analysis of Takeuchi and co-workers [21]. ΔS_{mix} is given by the sum of the configurational entropy ΔS_{conf} and the mismatch entropy ΔS_{mis} , which is a function of the mismatch between the atomic sizes of the components. Calculations were performed with a temperature of 1000K, slightly above the melting temperature of aluminium ($T_m = 933$ K). We found the difference between the two alloys in $\Delta H_{mix} = -0.5$ kJ/mole and the difference in $T\Delta S_{conf} = 1.0$ kJ/mole, while the contribution of ΔS_{mis} was negligibly small. We conclude from this result that the main thermodynamic driving force for the increase in GFA by substitution of Ni by Co and of Y by La is the configurational entropy.

The influence of the element substitution on the kinetics of glass formation is less clear. The improved GFA for the 5-component alloy must be related to higher viscosity. According to the free volume theory [22] the viscosity of liquids depends on the atomic volume. Substitution of elements by those of the same size will therefore not change the viscosity of the (undercooled) liquid. The difference in viscosity must therefore be due to the small differences in the electronic properties.

In conclusion, our results reveal strong shortening of Ni-Al and Co-Al bonds and a related small number of nearest neighbours. This behaviour is ascribed to the pronounced covalent character of the Al-TM bonds. Applying the cluster line model to our results yields a composition which differs considerably from the composition given by Yang et al. [4, 5] suggesting that the cluster line model is not capable of predicting the composition with optimum GFA. The increase in GFA through substitution of Ni by Co is ascribed to the site substitution of Ni by Co in the amorphous structure. A quantitative estimation of the contributions of ΔH_{mix} and $T\Delta S_{conf}$ to ΔG_{mix} for the two alloys showed that the difference in configurational entropy between the two alloys is the main thermodynamic driving force for the improved GFA of the 5-component alloy.

Acknowledgement

We would like to thank C. Leistner for her help in specimen preparation. Financial support to one of the authors (Y. Liu) by a Chinese Scholarship Council is also gratefully acknowledged.

References

1. A. Inoue, K. Ohtera, A. P. Tsai, and T. Masumoto, *Jpn. J. Appl. Phys. Part II* **27**, L479 (1988).
2. G. Wilde, N. Boucharat, R. J. Hebert, H. Rösner, W. S. Tong, and J. H. Perepezko, *Adv. Eng. Mater.* **5**, 125 (2003).
3. H. Chen, Y. He, G. J. Shiflet, and S. J. Poon, *Nature* **367**, 541 (1994).
4. B. J. Yang, J. H. Yao, J. Zhang, H. W. Yang, J. Q. Wang, and E. Ma, *Scripta Mater.* **61**, 423 (2009).
5. B. J. Yang, J. H. Yao, Y.S. Chao, J. Q. Wang, and E. Ma, *Phil. Mag.* **90**, 3215 (2010).
6. H.W. Sheng, Y.Q. Cheng, P.L. Lee, S.D. Shastri, and E.Ma, *Acta Mater.* **56**, 6264 (2008).
7. K. Lonsdale, *International Tables for X-ray Crystallography*, Kynoch, Birmingham, England, 1968.
8. M. Newville, *J. Synchrotron Radiat.* **8**, 322 (2001).
9. B. Ravel, *J. Synchrotron Radiat.* **8**, 314 (2001).
10. J. J. Rehr, J. Mustre de Leon, S. I. Zabinsky, and R. C. Albers, *J. Amer. Chem. Soc.* **113**, 5135 (1991).
11. M. Matsuura, K. Asada, K. Konno, and M. Sakurai, *J. Alloys Compd.* **390**, 31 (2005).
12. T.A. Carlson, C.W. Nestor, T.C. Tucker, and F.B. Malik, *Phys. Rev.* **169**, 27 (127).
13. <http://www.webelements.com/yttrium/electronegativity.html>;
<http://www.webelements.com/lanthanum/electronegativity.html>.
14. F.R. de Boer, R. Boom, W.C.M. Mattens, A.R. Miedema and A.K. Nielsen, *Cohesion in Metals: Transition Metal Alloys*, North Holland (Amsterdam, 1988).
15. T. Egami and V. Vitek, in *Amorphous Materials: Modelling of Structure and Properties*, ed. by V. Vitek, TMS-AIME, Warrendale (1983) p. 127.
16. A.N. Mansour, C.P. Wong and R.A. Brizzolara, *Phys. Rev. B* **50**, 12401 (1994).

17. A.N. Mansour, A. Marcelli, and G. Cibin, *Phys. Rev. B* **65**, 134207 (2002).
18. K. Saksl, P. Jovari, H. Franz, Q.S. Zeng, J.F. Liu and J.Z. Jiang, *J. Physics: Condens. Matter* **18**, 7579 (2006).
19. W. Zalewski, J. Antonowicz, R. Bacewicz and J. Latuch, *J. Alloys Compd.* **468**, 40 (2009).
20. D. B. Miracle, *Nat. Mater.* **3**, 697 (2004).
21. A. Takeuchi and A. Inoue, *Materials Transactions, JIM* **41**, 1372 (2000).
22. F. Spaepen, *Acta Mater* **25**, 407 (1977).

Table 1

Parameters, obtained by fitting the one-shell model to the data. N : number of nearest neighbours; D : distance of nearest neighbours; σ^2 : mean squared relative displacement of the effective interatomic distance. For comparison, the sum of the atomic radii of the absorbing atom and the aluminium atom, $R^* = r_{TM} + r_{Al}$ determined by the use of atomic radii listed in Ref [7], the effective radii, r_{eff} , determined from the EXAFS measurements and from the use of the hard sphere model [13], as well as the number of nearest neighbours, N_{DRPHS} , assuming dense random packing of hard spheres, are listed.

	Absorbing atom	N	N_{DRPHS}	D (Å)	R^* (Å)	σ^2 (Å ²)	r_{eff} (Å)
$Al_{86}Ni_8Y_6$	Ni	6.3±0.2	10.9	2.45±0.01	2.68	0.0084±0.0007	Ni: 0.76 Al: 1.68
$Al_{86}Ni_6Co_2Y_{4.5}La_{1.5}$	Ni	6.2±0.3	10.9	2.44±0.01	2.68	0.0093±0.0008	Ni: 0.76 Al: 1.68
$Al_{86}Ni_6Co_2Y_{4.5}La_{1.5}$	Co	6.3±0.2	10.9	2.42±0.02	2.68	0.0083±0.0009	Co: 0.70 Al: 1.72

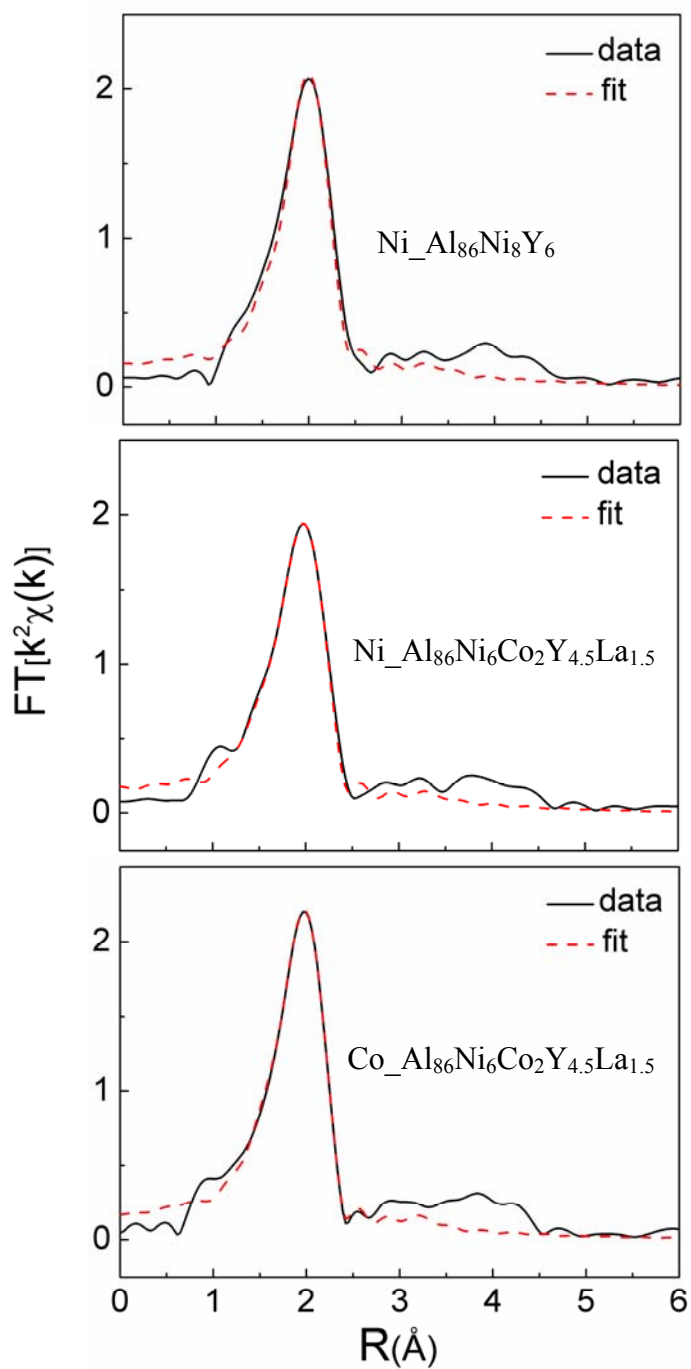


Fig. 1: Fourier Transform of the Ni EXAFS function of $\text{Al}_{86}\text{Ni}_8\text{Y}_6$ (top) and both Ni and Co EXAFS functions of $\text{Al}_{86}\text{Ni}_6\text{Co}_2\text{Y}_{4.5}\text{La}_{1.5}$ (middle and bottom) along with fits to the data which were done in the range $1.1 \text{ \AA} < R < 2.46 \text{ \AA}$.

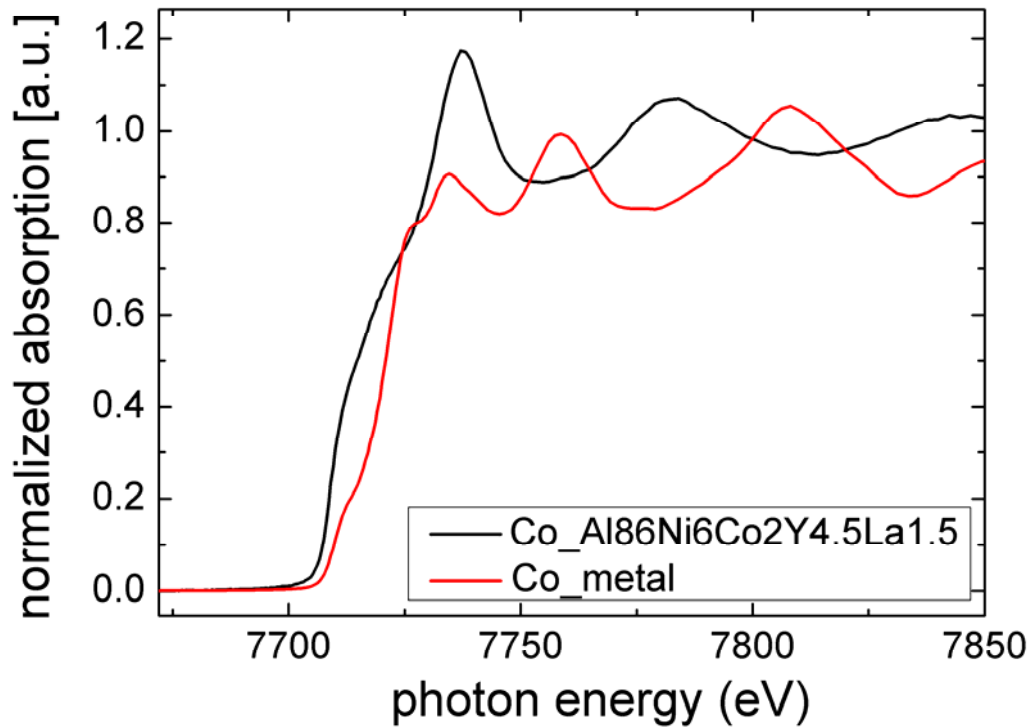
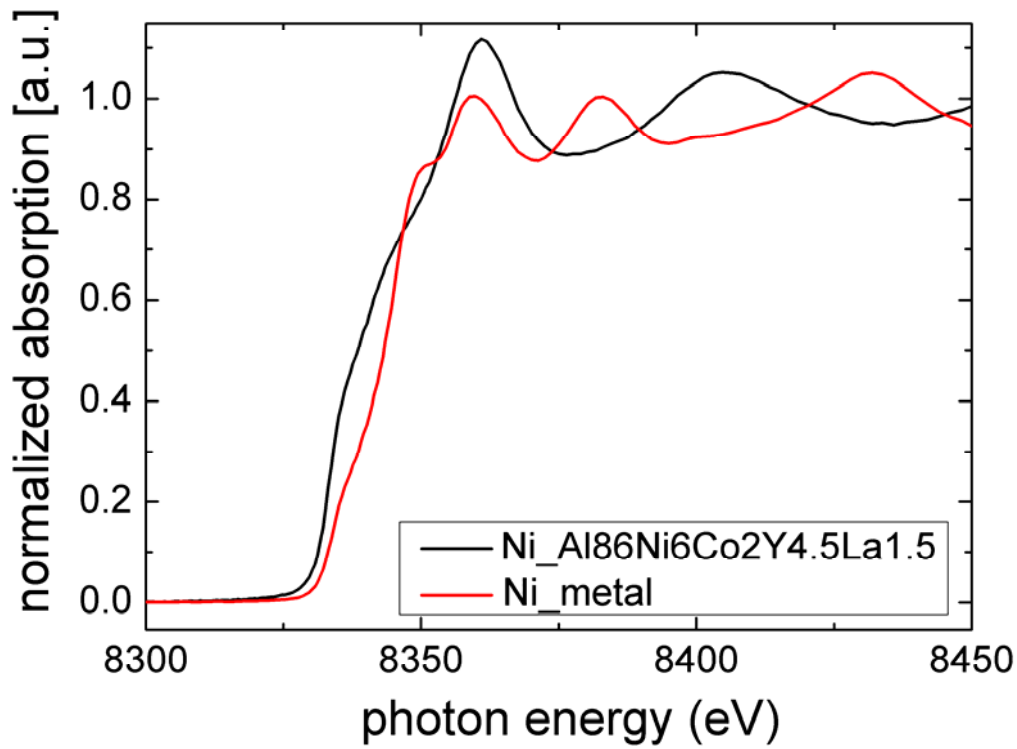


Fig. 2: Comparison of normalized Ni (a) and Co (b) K-edge XANES data for $\text{Al}_{86}\text{Ni}_6\text{Co}_2\text{Y}_{4.5}\text{La}_{1.5}$ BMG showing that the absorption edge for the alloy is shifted to lower energies compared to the pure element reference foil, indicating charge transfer from Al atoms of the first coordination sphere to Ni (a) and Co (b) atoms, respectively.